

Ruthenium(II) Complexes of Carboxylated Terpyridines and Dipyrazinylpyridines

Arta Stublla^[a] and Pierre G. Potvin^{*[a]}

Keywords: Ruthenium / Ligand effects / Density functional calculations / Carboxylation / Electronic structure

One-pot preparations of carboxylated 2,2';6',2''-terpyridine and 2,6-dipyrazin-2-ylpyridine ligands are reported in free acid and ester forms, as well as their transformations to homoleptic Ru^{II} complexes in very good yields. Density functional theory calculations of their geometry-optimized structures enabled their comparison with crystal structures; although the gross features of the crystal structures were reproduced, they showed much variability and distortion. The spectroscopic and electrochemical properties were analyzed from the point of view of their geometry-optimized struc-

tures, molecular orbital characteristics and electronic transitions, specifically to assess the effects of carboxylation and of inserting a phenylene spacer between the tridentate portion and the carboxyl group. The dipyrazinylpyridine complexes had HOMO levels stabilized by approximately 1 eV relative to the terpyridine analogues, and showed positive-shifted electrochemical potentials and redshifted electronic absorptions. Phenylene spacers were found to act as electron-donating groups, and the lowest-energy UV/Vis transitions showed intraligand character.

Introduction

Carboxylated Ru^{II} complexes are of interest in several contexts. We have reported how carboxyl groups can supramolecularly assist electron transfers from a photoexcited complex to a cationic electron acceptor.^[1] The Hanan group used carboxyl groups on such complexes to bridge Rh^I dimers in unique multinuclear assemblies.^[2] Constable et al. studied the solid-state hydrogen-bonding organization of two examples.^[3] We also have an interest in using carboxylated Ru^{II} complexes and their derivatives in the self-assembly of linear oligomers.

However, carboxylated complexes of Ru^{II} are currently of greatest interest as photovoltaic sensitizers, with so-called N3 and “black dye” as the best known examples.^[4] In this context, the carboxyl groups serve to anchor the complexes to the surfaces of the photoelectrodes, most commonly consisting of semiconducting anatase (TiO₂) coatings on indium/tin oxide conducting glass. The carboxyl groups are also expected to affect the electronic structures of the complexes and, by extension, their electrochemical and photophysical properties and, therefore, the driving force for electron injection, as well as the degree of electronic coupling between sensitizer and conduction band. Parsing those effects is not a simple matter.

Unless a ligand is attached to the electrode surface, its photoinduced dissociation is a concern with respect to the long-term stability of photoelectrodes and, in this regard, tridentate ligands are preferred over bidentate ones. They are, moreover, nonstereogenic. However, terpyridine (tpy) complexes have notoriously short excited-state lifetimes in comparison with their bidentate analogues, as exemplified by the parent complexes [Ru(tpy)₂]²⁺ (sub-nanosecond timescale)^[5] and [Ru(bpy)₃]²⁺ (millisecond timescale; bpy = bipyridine).^[6,7] Pyrazine-containing ligands have long been known,^[8] but the first dipyrazinylpyridine (dpp) was reported in 2001,^[9] and we found that its homoleptic Ru^{II} complex showed a longer excited-state lifetime than its terpyridine analogue and faster rates of photoinduced electron transfer in homogeneous solution.^[10] This was attributed mainly to the presence of the additional nitrogen atoms. The electron injections from photoexcited states into a conduction band of a semiconductor have been found to be extremely rapid (femtosecond timescale),^[11] and this would seem to diminish the importance of the excited-state lifetime. Nevertheless, electron-withdrawing appendages have been used to lengthen the lifetimes, albeit with a lower net exploitable excited-state energy.

To address some of these questions, we have launched a limited but systematic study of carboxylated Ru^{II} complexes of terpyridines and dipyrazinylpyridines and their ester derivatives, with and without a spacer separating the carboxyl groups from the core ligand to mitigate the electronic impact of carboxylation. This will entail studies of homoleptic and heteroleptic sensitizers, in solution as well as adsorbed on surfaces. We report here the preparation of carboxylated terpyridine and dipyrazinylpyridine ligands and their

[a] Department of Chemistry, York University,
4700 Keele Street, Toronto, ON M3J 1P3, Canada
Fax: +1-416-736-5936
E-mail: pspotvin@yorku.ca

Supporting information for this article is available on the WWW under <http://dx.doi.org/10.1002/ejic.201000122>.

homoleptic complexes, their spectroscopic and electrochemical characterization in solution, and analyses based on relevant electronic structure computations using density functional theory (DFT).

Results and Discussion

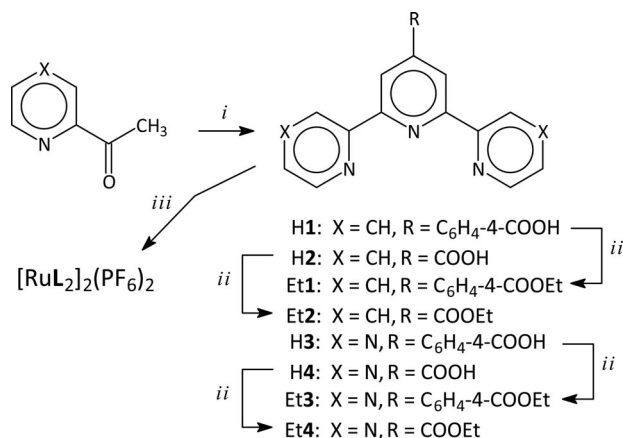
Synthesis

Some of the terpyridine materials described here have been reported previously or were reported during the course of our own work, although the yields, the synthetic ease, the ease of isolation and the levels of characterization that have been reported were not always satisfactory. None have previously been fully characterized in terms of spectral and electrochemical properties. The dpp materials reported are all new. There are two general approaches that have been followed in the preparation of Ru^{II} complexes of carboxylated terpyridines, either by direct synthesis from the free ligands or by the modification of precursor complexes, and our work has used both approaches.

The terpyridinylbenzoic acid **H1** has been prepared in 18% yield in boiling acetamide,^[12] and was reported as the dmsolvate of the HBr disalt. It was later prepared by a two-step Kröhnke method, with the second step proceeding in 65% yield (first step not described), and incorporated into an Ir^I complex.^[13] A third preparation used a process similar to ours (49% yield) and converted **H1** to neutral, zwitterionic Ru(1)₂ (66% yield),^[3] the pentahydrate of which was characterized by using crystallography. Finally, the ligand has been prepared by base hydrolysis (93% yield)^[14] of the methyl ester, itself obtained in two steps (15% yield),^[15] and incorporated into a heteroleptic Ru^{II} species. We had earlier prepared both homo- and heteroleptic Ru^{II} complexes of **H1** by KMnO₄ oxidation of the corresponding homoleptic 4'-(*p*-tolyl) complex, albeit as a mixture requiring chromatography, in low yields of each, and in an incompletely characterized state.^[1] In accord with Constable et al.,^[3] part of the difficulty we encountered in manipulating these products was their variable protonation state. The methyl ester of **H1** (**Me1**) has also been prepared in 25% yield after 8 d.^[3] Using microwave irradiation in high-boiling solvent, Constable et al. converted this ester to its homoleptic Ru^{II} complex, [Ru(**Me1**)₂]²⁺, isolated as the PF₆⁻ disalt in 73% yield. Alternatively, autoclave reaction of the ester in MeOH at 150 °C provided the dichloride salt (66% yield), characterized as a pentahydrate by using elemental analysis but as a tetrahydrate by using crystallography. The PF₆⁻ salt was hydrolyzed to a variable mixture of [Ru(**H1**)₂]²⁺ and [Ru(1)(**H1**)]⁺ (61% yield) lacking confirmation by elemental analysis.^[3] Heteroleptic Ru^{II} complexes of **H1** have also been described.^[2,14]

In this work, we used a one-pot synthesis of **H1** at room temperature from 2-acetylpyridine and 4-carboxybenzaldehyde (the ethyl ester of which can be used just as well) in the presence of KOH and NH₄OH in aqueous MeOH (Scheme 1), a process that we have previously used to prepare several 4'-substituted terpyridines and dipyrazinylpyri-

dines.^[9,10,16,17] This precipitates a salt form which, after redissolving, was acidified to precipitate analytically pure **H1** in 80% yield. The salt form was also transformed to the ethyl ester **Et1** by standard Fischer esterification in 70% yield. To prepare the corresponding complexes, RuCl₃ was pre-activated with AgBF₄ in dmf, then treated with the ligand to afford, after precipitation by anion exchange, pure [Ru(**H1**)₂](PF₆)₂ (95% yield) or [Ru(**Et1**)₂](PF₆)₂ (98% yield).



Scheme 1. Ligand synthesis: (i) OHCC₆H₄-4-COOH or OHCCOOEt, 15% KOH, concd. NH₄OH/CH₃OH/H₂O (1:1)/r.t./3 d; then dilute HCl; (ii) EtOH, concd. H₂SO₄/reflux/2.5–3 d; (iii) (a) RuCl₃, AgBF₄/dmf/reflux/3 h; (b) add L/reflux/3 d; (c) excess amount of NH₄PF₆/H₂O.

The free ligand lacking the spacer, terpyridine-4'-carboxylic acid **H2**, was first isolated as an unintended byproduct of a convergent preparation of its ethyl ester by Stille coupling, in 4 steps and 28% overall yield from commercial citrazinic acid.^[18] Later, **H2** was prepared by means of 4- and 5-step processes featuring two methods of oxidizing 4'-methylterpyridine, in 18 and 16% yields, respectively, then converted to [Ru(**H2**)₂]²⁺ in 55% yield by heating with [Ru(dmsolv)₄Cl₂], but none of the products or intermediates were characterized by anything more than ¹H NMR spectroscopy and sometimes MS.^[14] Constable et al. prepared [Ru(**H2**)₂]²⁺ in 48% yield by oxidative degradation of a 4'-furyl precursor, which itself was available in 86% yield.^[3] This novel approach was based on earlier work by Beley et al.,^[19] who prepared a heteroleptic Ru^{II} complex of **H2** by means of a similar oxidation. These authors had also prepared the same complex directly from **H2**, but only in 6% yield, as well as by hydrolysis of the ester analogue. That process was sluggish (18% yield) and was accompanied by ligand scrambling to also afford [Ru(**H2**)₂]²⁺ as one of two byproducts (3% yield), but none of these materials was completely characterized. The fully deprotonated Ru(2)₂ resulted from an attempt to prepare a coordination polymer from [Ru(**H2**)₂]²⁺ and Zn²⁺, and was only characterized by crystallography as the tetrahydrate.^[3]

In a similar fashion to that for **H1**, we prepared **H2** in one step from 2-acetylpyridine and ethyl glyoxylate and isolated it as the hydrochloride salt in 60% yield. Conversion

of the ester Et $2^{[28]}$ to [Ru(Et 2) $_2$](PF $_6$) $_2$ as before was uncomplicated (82% yield) but not so with H 2 . The direct reaction to produce [Ru(H 2) $_2$](PF $_6$) $_2$ worked well and provided high-purity material, the ^1H NMR spectra of which matched those reported,^[3,14] but drying the product to prepare an analytical sample resulted in a partial loss of HPF $_6$, whereby the material turned a darker shade of red and became insoluble in common solvents. A reliable measure of the yield was therefore not possible. This precipitation was reversed by stirring with aqueous HPF $_6$ but no water-free sample could be prepared in this way. Instead, [Ru(H 2) $_2$](PF $_6$) $_2$ was obtained analytically pure and water-free by base hydrolysis of [Ru(Et 2) $_2$](PF $_6$) $_2$ and precipitation with acid (100% yield).

By following the same one-pot procedure as that for H 1 and H 2 , the new ligands H 3 and H 4 were obtained from 2-acetylpyrazine in 80 and 55% yields, respectively. Conversion to Et 3 (76% yield), [Ru(H 3) $_2$](PF $_6$) $_2$ (58% yield), [Ru(Et 3) $_2$](PF $_6$) $_2$ (30% yield) or [Ru(H 4) $_2$](PF $_6$) $_2$ (38% yield) was uncomplicated. As was the case with H 2 , a direct preparation of [Ru(H 4) $_2$](PF $_6$) $_2$ provided material that had ^1H NMR spectra consistent with the structure, but the elemental analyses were not. Instead, [Ru(H 4) $_2$](PF $_6$) $_2$ was obtained analytically pure by base hydrolysis of [Ru(Et 4) $_2$](PF $_6$) $_2$ and precipitation with acid (38% yield).

The yields of these dpp materials were generally lower than those of terpyridine analogues, which we ascribe to the generally lower reactivity of dipyrazinylpyridines in forming complexes, as well as difficulties in purifying and handling the products. Although [Ru(Et 3) $_2$](PF $_6$) $_2$ was obtained essentially pure without chromatography, an analytically pure sample was obtained after preparative TLC. All of the carboxylic acid complexes tended to lose the elements of HPF $_6$ while in solution, as noted with other deprotonatable complexes,^[1,20,21] turning darker and becoming insoluble, but were redissolvable upon stirring with aqueous HPF $_6$.

All products were characterized by a combination of ^1H and ^{13}C NMR spectroscopy, IR spectroscopy, MS and elemental analysis for new materials. The complete NMR spectroscopic signal assignments, supported by 2D experiments, and the structures assigned to the mass spectral ions appear in the Supporting Information.

The EI-MS mass spectra of the free ligands and their esters showed the molecular ions and the expected fragment ions. The monocation-selective LDI-TOF mass spectrometric technique was used for the complexes, which all exhibited the expected isotopic clustering at m/z values that were in agreement with the assigned ion structures. The highest-mass clusters were variably of formula [M - 2 PF $_6$] $^+$, [M - PF $_6$] $^+$ or [M] $^+$. With [Ru(H 1) $_2$] $^{2+}$ and [Ru(H 2) $_2$] $^{2+}$, overlapping clusters of ions differing by one mass unit were found. In addition, the complexes yielded cascades of fragment ions from the predictable losses of side-chain components.

Because of their zwitterionic nature, the carboxylic acid complexes were not soluble in ordinary solvents, so their NMR spectra were acquired in deuterated trifluoroacetic acid ([D]tfa) and thus reflect partially protonated forms. The ^1H NMR spectroscopy of (terpyridine)Ru II complexes

has been amply described in the literature, and the relatively simple spectra obtained with our high-symmetry complexes will not be detailed here, apart to report that they showed the diagnostic upfield shift of the narrow 6/6''-H doublets and 5/5''-H doublets of doublets upon complexation, owing to the magnetic anisotropy of the perpendicular ligand. The ^1H NMR spectroscopy of dipyrazinylpyridines differs from that of terpyridines because of small coupling constants, such that the aromatic signals can appear as broad singlets at low resolution, and at generally more downfield positions. The ^{13}C NMR spectra of Ru II complexes are rarely reported but were obtained for all species. For both ligands and complexes, these were consistent with the structures and, by use of distortionless enhancement by polarization transfer (DEPT), heteronuclear single quantum coherence (HSQC) and heteronuclear multiple bond correlation (HMBC) pulse sequences, all ^{13}C NMR spectroscopic signals were assigned. Because the spectra were not all obtained in the same solvent, comparisons between them must be made with caution. In comparing the spectra of the esterified species, the ^{13}C NMR spectroscopic signals generally migrate downfield upon complexation (by up to 3.8 ppm), including those for C-6/6'' and C-5/5''. In other words, the magnetic anisotropy felt by 6/6''-H and 5/5''-H was not felt as strongly by the attached carbon nuclei. The only exceptions were upfield-migrating signals from those carbon atoms lying along the symmetry axes of the ligands (through C-4' and on the side-chain), by 0.3–2.1 ppm, as well as those for the methyl carbon atoms (by 0.7 ppm) but not the CH $_2$ carbon atoms. Analogous changes were found in comparison of the spectra of free carboxylic acid ligands and their complexes, although additional changes were attributable to the partially protonated states of the free ligands.

Molecular Structure

The complexes reported here were red, microcrystalline and stable as solids, but all attempts at crystal growth were unsuccessful. In particular, the prolonged standing of solutions of the carboxylic forms resulted in the deposition of insoluble and powdery deprotonated forms, and the crystal structures of the deprotonated forms Ru(1) $_2$ or Ru(2) $_2$ have already been reported.^[3] Therefore, DFT-optimized structures were obtained for all the complexes reported here, and these provided insights into their electronic structures (see below). Except for the obvious differences owing to the replacement of pyridine rings with pyrazine rings, the structures of the dpp complexes were virtually the same as those of the terpyridine analogues. The Supporting Information reports some measurements. The crystal structures of six relevant terpyridine complexes^[2,3] also gave us the opportunity to compare solid-phase and computed structures.

In terms of the flatness of the tridentate moieties, there was an important difference. All six crystal structures showed deviations in the coplanarity of the three pyridine rings in each terpyridine ligand (pyridine planes twisted by

up to 7°), which has been noted in earlier examples of terpyridine complexes.^[22] This was most pronounced with $\text{Ru}(\mathbf{2})_2$, and was coupled to a strong bowing of the meridional planes by the Ru–pyridine–phenylene–carboxylate sequences, no doubt because of packing pressures. In the DFT-calculated structures of our complexes, any such deviation from terpyridine coplanarity was very slight (1° or less). There was no evident sign of a particular distortion of the computed pyridine–pyridine linkages to accommodate the greater coplanarity, neither in the interpyridine bond lengths, nor in the N–C–C–N, N–C–C–C or N–C–C angles. However, the interpyridine C3–C3' and C5'–C3'' distances were more variable but noticeably shorter in the crystal structures ($3.070 \pm 0.016 \text{ \AA}$) than in the computed ones ($3.107 \pm 0.004 \text{ \AA}$). These shorter distances will translate into stronger steric repulsions between the attached hydrogen atoms and greater interplanar twisting, but this was perhaps avoided in the computed structures by the cumulated effects of several unremarkably small bond and angular distortions. On the other hand, DFT systematically overestimated the Ru–N bond lengths, but only by about 0.04 \AA .

There were some differences in the amount of twisting by the phenylene and carboxyl groups out of coplanarity with the rings to which they are attached, some of which can be ascribed to secondary interactions and crystal packing. The four crystallographically unique ligands of $[\text{Ru}(\text{Me}1)_2]\text{Cl}_2 \cdot 4\text{H}_2\text{O}$ ^[3] had half of the phenylene side chains rotated $36.2\text{--}39.6^\circ$ from the planes of the attached pyridines, whereas those of the other half were essentially coplanar (interplanar angles $4.4\text{--}5.3^\circ$), apparently stabilized by π stacking with the pyridine rings on a neighbouring complex of the unit cell, as well as by agostic H– π interactions ($2.75\text{--}3.00 \text{ \AA}$) between a phenylene hydrogen atom and a pyridine ring belonging to the perpendicular ligand on that same neighbour. There were also hydrogen-bonding networks involving the C=O groups, the anions and water molecules that imposed some distortions, but the ester COO moieties were essentially coplanar with the attached phenylene groups (interplanar angles $2.0\text{--}8.8^\circ$) in all four crystallographically unique ligands. The computed structures of the Et1 and Et3 analogues differed in that the phenylene and central pyridine rings were strongly twisted ($30.0\text{--}31.9^\circ$), and the carboxy and phenylene planes were also twisted by similar amounts ($32.8\text{--}33.2^\circ$), but in the opposite direction such that the carboxy moieties were virtually parallel with the central pyridine rings. This appears to give rise to communication between these groups (see below). The crystal structure of $\text{Ru}(\mathbf{1})_2 \cdot 5\text{H}_2\text{O}$ ^[3] showed smaller twists (phenylene–pyridine interplanar angles $18.7\text{--}29.1^\circ$, phenylene–COO interplanar angles $10.1\text{--}17.0^\circ$). In contrast, the COOH groups in the calculated H1 and H3 structures were virtually parallel with the spacers. Hydrogen-bonding networks may have been responsible for the lack of coplanarity in the crystal. The crystal structures of three mixed-ligand complexes of H1 were variable: The COOH group was coplanar in $[\text{Ru}(\text{H1})(\text{phtpy})]^{2+}$ (phtpy = 4'-phenyl-2,2';6',2''-terpyridine) but twisted in $[\text{Ru}(\text{H1})(\text{tpy})]^{2+}$ and

in an $[\text{Ru}(\mathbf{1})(\text{tpy})]$ -linked Rh dimer.^[2] Both crystalline $[\text{Ru}(\mathbf{2})_2] \cdot 4\text{H}_2\text{O}$ ^[3] and the computed structures of H2 and H4 showed analogous twists of the COO moieties relative to the central pyridine ring.

There were additional small distortions: Some examples showed an in-plane bend of the pyridine-to-carboxyl or phenylene-to-carboxyl linkages off the central axis by $2\text{--}3.5^\circ$, perhaps to accommodate the OH/OEt bulk. Several showed a bend of these linkages off the attached pyridine or phenylene planes (by up to 0.141 \AA at the carboxyl carbon atoms). This was most severe with the benzoate esters. Similar bends by up to 0.142 \AA were also found in the crystal structures. As the side chains are not symmetrical, and in any case twisted, bent in-plane and sometimes out-of-plane, the tridentate cores themselves are also unsymmetrical, but the bond-length differences between otherwise equivalent bonds within any one tridentate moiety were small (at most 0.007 \AA , but averaging $< 0.0003 \text{ \AA}$).

Comparison between the crystalline $\text{Ru}(\mathbf{1})_2$ and $\text{Ru}(\mathbf{2})_2$ ^[3] reveals that the insertion of a phenylene spacer caused each of the central pyridine bonds to lengthen, on average by $(0.013 \pm 0.004) \text{ \AA}$ (C4'–C3'/5'), $(0.007 \pm 0.008) \text{ \AA}$ (C2'/6'–C3'/5') or $(0.012 \pm 0.006) \text{ \AA}$ (C2'/6'–N). Only the first of these changes is statistically significant, and with only one such comparison available between species under crystal-packing pressures and showing high bond-length variability, no definitive conclusion can be drawn. In contrast, the DFT structures were more consistent. Introduction of a spacer lengthened the C-4'–C-3'/5' bonds by $(0.011 \pm 0.001) \text{ \AA}$, in accord with what was found in the crystal structures, whereas all other central pyridine bonds were shortened by an average $(0.002 \pm 0.0005) \text{ \AA}$. Comparison with the unsubstituted parent complexes, $[\text{Ru}(\text{tpy})_2]^{2+}$ and $[\text{Ru}(\text{dpp})_2]^{2+}$,^[17] revealed that adding a COOH or COOEt appendage caused weaker changes to these bond lengths, on the order of 0.003 \AA or less. This is consistent with the relatively strong effects of phenylene groups on orbital energies (see below).

Importantly, metal binding caused little change in the interplanar twists: within a few degrees, the computed structures of the free ester ligands had the same side-chain orientations as in the complexes. Metal binding to the ligands caused bond-length changes that stretched throughout the full length of the side chains (see the Supporting Information). There were bond elongations and compressions in alternation within the central pyridine rings, which, in the Et1 case, were coupled to the phenylene spacer being drawn in, and furthermore, compressed along the central axis, suggestive of an overall shift of phenylene electron density toward the metal atom. With or without a spacer, the ester portions were at the same time drawn away from the metal atom, suggestive of a decreased ester-to-pyridine coupling, balanced by what appears to be an increased overlap of the ethoxy oxygen atom with the carbonyl group. There were also changes in atomic charge (see the Supporting Information), namely, increases in positive charge (or reductions of negative charge) at all positions of the central pyridine ring and stretching out to the ester groups as well, similar

in both ester cases, with the notable exceptions of the charges on the carboxyl carbon atoms and the phenylene C-4 atom (linked to the pyridine C-4' atom), which became more negative. Unfortunately, neither bond-length changes nor atomic-charge shifts provided a ready, consistent explanation for the complexation-induced upfield migrations of the NMR spectroscopic signals from the carbon atoms lying on the C_2 axis.

Electronic Structure

Figure 1 presents the calculated frontier orbital compositions for $[\text{Ru}(\text{H1})_2]^{2+}$ and $[\text{Ru}(\text{H3})_2]^{2+}$, which are illustrative of most of our complexes, and Figures 2 and 4 (below) show a comparison of the energy levels of the frontier orbitals for all of the new complexes with those of the unsubstituted analogues $[\text{Ru}(\text{tpy})_2]^{2+}$ and $[\text{Ru}(\text{dpp})_2]^{2+}$.

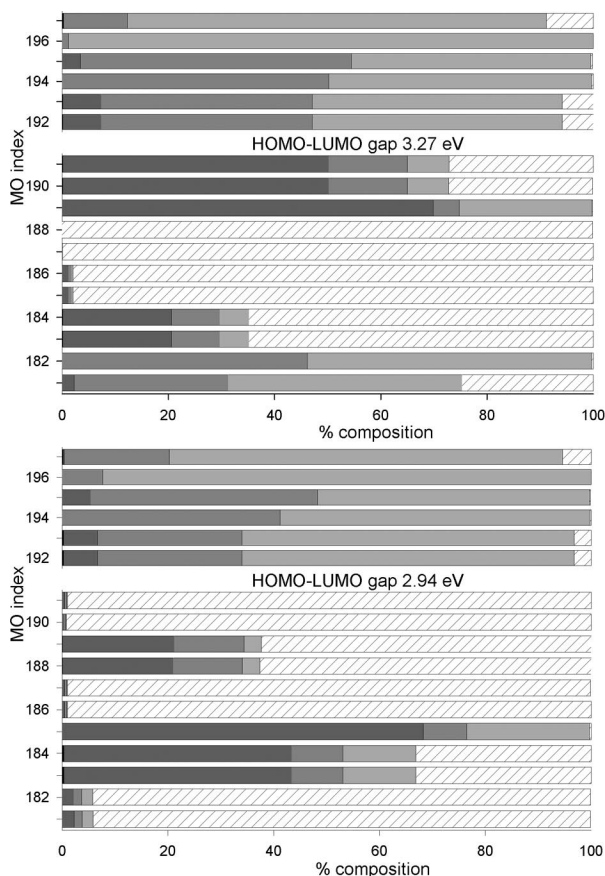


Figure 1. Frontier orbitals of $[\text{Ru}(\text{H1})_2]^{2+}$ (top) and $[\text{Ru}(\text{H3})_2]^{2+}$ (bottom) decomposed into contributions from Ru s and p (black), Ru 4d (dark grey), the central pyridine (medium grey), outer pyridine/pyrazine ring (light grey) and side chain (hashed) orbitals.

For the H1 species, the three highest-energy occupied orbitals, two of which are nearly degenerate, are mixed but with much Ru t_{2g} character, and these are followed by a suite of side-chain π -type orbitals, including two nearly degenerate pairs, showing little mixing with pyridine π levels, as expected given the significant twist angle (Figure 2). Yet, as Figure 3 shows, some occupied orbitals have contri-

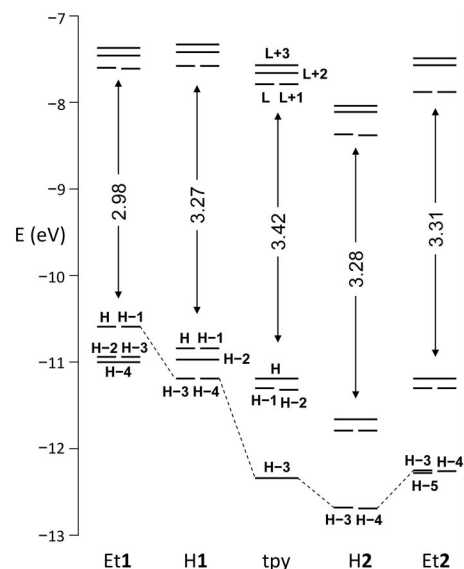


Figure 2. Frontier orbital energy levels (H stands for HOMO and L for LUMO) and HOMO–LUMO gaps (in eV) in homoleptic complexes of the indicated ligands. The dotted lines join the highest-lying ligand-centred π orbitals. The LUMO patterns are the same for all species, and the upper three HOMO levels (mainly t_{2g}) appear in the same order with tpy, H2 and Et2.

butions from both terpyridine and carboxylate moieties without significant mediation by the phenylene rings. The orbital compositions for the H2 species (see the Supporting Information) are similar: the three highest-energy HOMO levels are less mixed than in the H1 case and are mainly of Ru t_{2g} character, but with only two high-lying orbitals (HOMO–3 and HOMO–4) possessing much side-chain character, as expected for the smaller substituent. In both complexes, the two lowest LUMO levels are nearly degenerate and contain some metal and side-chain character, but the lowest four are all principally of pyridine π^* type. When compared to the corresponding situation in $[\text{Ru}(\text{tpy})_2]^{2+}$, Figure 2 reveals that the COOH group in the H2 complex stabilizes to a greater extent the LUMO levels than the HOMO levels, narrowing the HOMO–LUMO gap somewhat; it thus acts as a typical electron-withdrawing substituent.

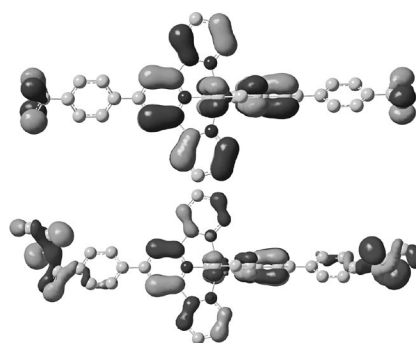


Figure 3. Images of HOMO–10 in $[\text{Ru}(\text{H1})_2]^{2+}$ (top) and HOMO–11 in $[\text{Ru}(\text{Et1})_2]^{2+}$ (bottom) showing electron density bypassing the twisted phenylene spacers. Note the coplanarity of the COOH group and the non-coplanarity of the COOEt group with the phenylene spacer.

ent, even if not coplanar. In contrast, the carboxyphenyl groups in $[\text{Ru}(\text{H1})_2]^{2+}$ raised the metal-centred HOMO levels and, to a lesser extent, the pyridine-centred LUMO levels, such that the HOMO–LUMO gap was slightly narrowed; it thus acts as a typical electron-donating substituent in spite of the attached, coplanar COOH.

One difference between the H1 and H2 cases is that the lowest two LUMO levels have a greater total contribution from the outer pyridine rings in the former, whereas they are centred mostly over the central pyridine ring in the latter case. This difference is consistent with the different electronic effects of the two side chains.

The frontier orbital compositions for the Et2 complex closely mimic those of its carboxylic acid parent, but the levels are shifted up in energy, essentially cancelling out the effect of the COOH group. This is in accord with the ester having a less electron-withdrawing C=O group, even though it was rotated into coplanarity. The Et1 case is more complex. The phenylene–pyridine twists are identical in both the H1 and Et1 cases, but the carboxyl group of the H1 complex is parallel to the phenylene plane, whereas it is twisted out of plane in complexed Et1 to lie virtually parallel to the central pyridine ring. Here, too, some occupied ligand-centred orbitals reveal a terpyridine–carboxylate overlap that bypasses the phenylene ring (Figure 3). Presumably, the poorer phenylene–C=O overlap caused the energy of the two highest-lying and nearly degenerate phenylene-centred MOs to lie above those of the H1 case and become the nominal HOMO and HOMO–1 levels, with a substantially narrower calculated HOMO–LUMO gap resulting. Thus, in comparison with $[\text{Ru}(\text{tpy})_2]^{2+}$, the side chain of Et1 also behaves as a typical electron-donating group, but the LUMO and metal-centred HOMO levels were lower in energy than those with H1. There were no significant differences between the H1 and Et1 complexes in any of the bond lengths involving the metal atom, the terpyridine or the phenylene atoms, and the only significant differences in atomic charges occurred at the phenylene atoms.

For the dpp analogues, the frontier orbitals are about 1 eV lower in energy than in terpyridine analogues because of the added nitrogen atoms. The situation with the H4 species (see the Supporting Information) was otherwise similar to that of H2: the three highest-energy occupied orbitals are close in energy (two are nearly degenerate) and are mostly of Ru t_{2g} character; these are followed by two nearly degenerate side-chain π -type orbitals, showing little mixing with pyridine or pyrazine π levels owing to the significant twist angle, and then these are followed by four orbitals of mostly pyrazine π character. The LUMO and LUMO+1 levels are also nearly degenerate and show small contributions from metal and side-chain orbitals, but along with LUMO+3 and LUMO+4, have mostly pyridine and pyrazine π^* character. Here, too, a comparison with the corresponding situation in $[\text{Ru}(\text{dpp})_2]^{2+}$ shows that the COOH group acts as an electron-withdrawing substituent.

The LUMO levels are very much the same in the three other dpp complexes, but the HOMO levels for the H3 spe-

cies (Figure 4) are not at all similar to the H4 case: As with H1, the insertion of a phenylene spacer raised all of the frontier orbital energies, and introduced many side-chain-centred orbitals among the highest-energy occupied ones. The phenylene spacer therefore acts as an electron-donating group, but much more dramatically so than in the tpy analogue, with a much narrower HOMO–LUMO gap. Indeed, six of the eleven highest-energy HOMO levels are almost totally side chain in origin (HOMO, HOMO–1, HOMO–4, HOMO–5, HOMO–9, HOMO–10). The Ru t_{2g} character is more distributed, with HOMO–2 and HOMO–3 having only 21% and with more significant amounts lodged in deeper orbitals (HOMO–6 to HOMO–8).

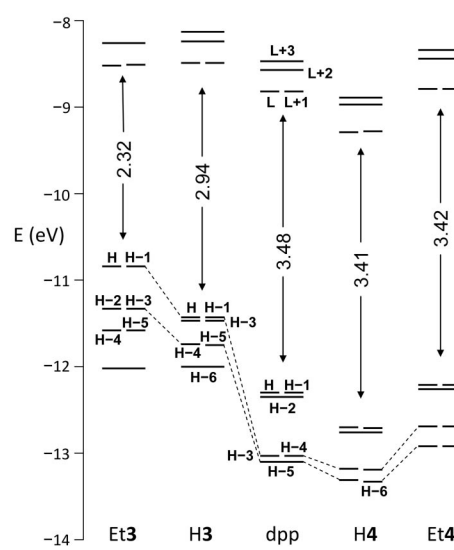


Figure 4. Frontier orbital energy levels (H stands for HOMO and L for LUMO) and HOMO–LUMO gaps in homoleptic complexes of the indicated ligands. The dotted lines join the highest-lying ligand-centred π orbitals. The LUMO patterns are the same for all species, and the upper three HOMO levels (mainly t_{2g}) appear in the same order with dpp, H4 and Et4.

In both of the H3 and H4 cases, the six lowest LUMO levels have a greater total contribution from the pyrazine rings than from the pyridine rings, in accord with the expectation that the extra nitrogen atom of a pyrazine ring would cause its π^* levels to be lower in energy than those of a pyridine ring and shift the principal electron sink from the central pyridine ring (as it is in terpyridines) to the outer pyrazine rings. These orbitals have more pyridine character in H4 than in H3, presumably because the electron-withdrawing COOH group of H4 stabilizes the π^* levels of the pyridine ring, thus increasing its contribution to the lowest unoccupied orbitals and resulting in a more distributed electron sink.

As was the case with Et2 relative to H2, the frontier orbitals of the Et4 complex closely mimic those of the H4 complex, with the levels shifted higher in energy due to esterification. Esterification of the H3 complex caused the LUMO and metal-character HOMO levels to decrease in energy. Otherwise, the lowest LUMO levels were virtual reproductions of those of its carboxylic acid analogue. Esteri-

fication to Et3 also caused a destabilization of the side-chain π levels, such that the uppermost four HOMO levels are almost purely side chain in character. As was the case for the tpy analogues, the optimized structure of $[\text{Ru}(\text{H3})_2]^{2+}$ placed the COOH group coplanar with the spacer, but the ester group of $[\text{Ru}(\text{Et3})_2]^{2+}$ was rotated out of coplanarity. This no doubt reduced the π -withdrawing ability of the C=O group, giving the phenylene spacer higher-energy π levels. At the same time, the lowering of the LUMO and metal-character HOMO levels would appear to reflect an increase in electron withdrawal by the side chain, or a decrease in electron donation, although the phenylene-pyridine twist angle in the optimized structures actually decreased upon esterification.

Electronic Spectroscopy

UV/Vis absorption and electrochemical measurements were performed in CH_3CN to assess the effects of the substituents on the electronic properties of the complexes in comparison with noncarboxylated analogues. Table 1 reports the visible-region absorption maxima (λ_{MLCT}) and the measured half-wave potentials ($E_{1/2}$). Figure 5 presents representative UV/Vis spectra, with the corresponding time-dependent (TD)-DFT-calculated spectra overlaid for comparison. These were typical of this class of complex, with strong π - π^* bands in the 250–350 nm range, and dominated in the visible region by a metal-to-ligand charge transfer (MLCT) band near 490 nm. There was a higher-energy shoulder that reveals the contribution of more than one transition. Although the λ_{MLCT} positions were relatively independent of the substitution, all substituents caused a redshift relative to the λ_{MLCT} position reported for $[\text{Ru}(\text{tpy})_2]^{2+}$, which is consistent with prior findings and with our computation of narrower HOMO–LUMO gaps.

Table 1. Visible-region absorption maxima and redox potentials in CH_3CN of $[\text{RuL}_2]^{2+}$ complexes (see Experimental Section for conditions).

L	λ_{MLCT} [nm] (ϵ [$10^4 \text{ M}^{-1} \text{ cm}^{-1}$])	E^{ox}	$E_{1/2}$ [V] vs. SCE E^{red}
H1	491 (2.76)	+1.24	–1.28, ^[a] –1.5 ^[a]
Et1	491 (2.50)	+1.27	–1.15, –1.37, –1.74
H2	490 (3.10)	+1.37	–0.8, ^[a] –1.03, –1.40, –1.65
Et2	488 (2.97)	+1.43	–0.99, –1.21, –1.47
tpy ^[b]	476 ^[c]	+1.27	–1.27
H3	493 (0.625), 410 (sh.)	+1.72	(no clear waves)
Et3	495 (2.00), 409 (sh.)	+1.60	–0.88, –1.07, –1.40
H4	510 (2.00), 430 (sh.)	+1.83	(no clear waves)
Et4	483 (1.95), 406 (sh.)	+1.73	–0.76, –0.95, –1.36, –1.69
tdpp ^[d]	498 (1.66)	+1.62	–0.83, –1.04, ca. –1.30

[a] Irreversible process; peak cathodic potential (E_{pc}) reported. [b] From Morris et al.^[23] [c] From Hecker et al.^[24] [d] From Liegghio et al.^[9]

The gas-phase TD-DFT and experimental spectra were qualitatively the same in all cases, with the λ_{MLCT} values matching best for the complexes with phenylene spacers. In general, the HOMO–LUMO gaps were systematically overestimated except for the Et1 and Et3 complexes, for which

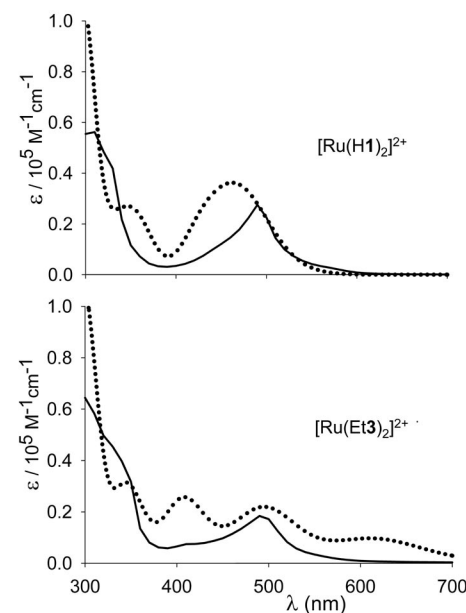


Figure 5. Experimental (solid lines) and TD-DFT calculated spectra (dotted lines, arbitrary scale).

the λ_{MLCT} values matched best. The transition assignments appear in the Supporting Information. In all cases, there are two transitions mainly responsible for the lowest-energy absorption envelopes. In the cases lacking a spacer, the least energetic transition is from degenerate HOMO/HOMO–1 (or HOMO–1/HOMO–2) of mainly t_{2g} character to degenerate LUMO/LUMO+1, and the higher-energy shoulder comes from the third, mainly t_{2g} level to the LUMO+2, all tridentate-centred. In the H1 and H3 complexes, however, the HOMO and HOMO–1 levels, which are almost totally side chain in character, contribute negligibly to the visible-region transitions. The same is true of HOMO–4 and HOMO–5. Instead, the lowest-energy transition originates from the mixed t_{2g} /side-chain orbitals (HOMO–2 and HOMO–3) to the usual LUMO levels, and the two transitions contributing to the higher-energy shoulder come from the other orbitals with relatively high metal character (HOMO–6 to HOMO–8) to these same LUMO levels. On the contrary, the main low-energy transition for the Et1 complex involved the side-chain-centred HOMO/HOMO–1 levels and is thus very much intraligand in character (phenylene π to mostly central pyridine π^*) as well as having MLCT character (Figure 6 illustrates this combined transition), whereas the higher-energy shoulder is a more classical MLCT transition. In the Et3 case, in which six of the eight highest-lying occupied orbitals are almost purely side chain in character, the main low-energy transition also had a strong intraligand character, whereas the new low-energy shoulder (calculated peak at 617 nm) is almost purely intraligand in character (phenylene π to mostly pyrazine π^* , also illustrated in Figure 6), originating from the four highest-lying, ligand-centred HOMOs.

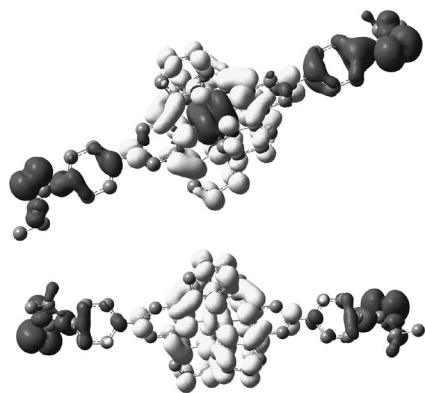


Figure 6. Kohn–Sham representation of the lowest-energy transitions in the UV/Vis spectra of $[\text{Ru}(\text{Et}1)_2]^{2+}$, which illustrates the combined metal-to-ligand and intraligand characters (top), and of $[\text{Ru}(\text{Et}3)_2]^{2+}$, which has pure intraligand character (bottom). Dark grey areas represent electron-density sources corresponding to combinations of HOMO to HOMO–3 (top) and HOMO to HOMO–1 (bottom). Light gray represents electron-density sinks (LUMO and LUMO+1).

Electrochemistry

Figure 7 presents representative cyclic voltammetry (CV) and differential pulse voltammetry (DPV) traces. CV showed one reversible or quasireversible oxidation wave assigned to the $\text{Ru}^{\text{III}}/\text{Ru}^{\text{II}}$ couple. As expected, the $E_{1/2}$ values of the dpp complexes were shifted positive from those of the tpy analogues, no doubt owing to the additional nitrogen atoms in the tridentate moiety.^[8,25] The free acid complexes showed poorly discernible reduction waves, whether in CH_3CN or in dmf – no reversible CV waves and no DPV reduction peaks were found in the **H1** case – but the ester complexes showed up to four reversible or quasireversible reduction waves attributable to ligand-centred processes.

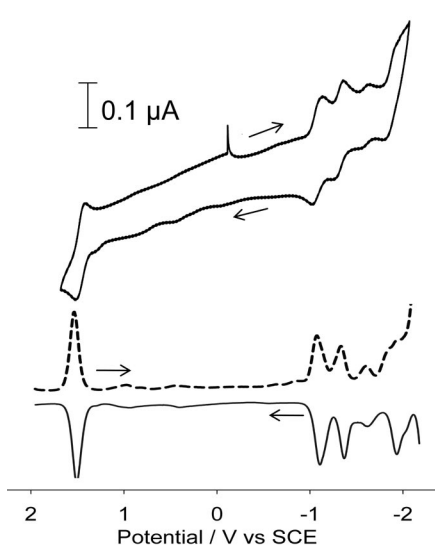


Figure 7. Cyclic voltammogram at 100 mVs^{-1} (top) and differential pulse voltammogram (bottom) of $[\text{Ru}(\text{Et}2)_2]^{2+}$ in CH_3CN containing 0.1 M TBAH.

In contrast to λ_{MLCT} , the $E_{1/2}$ values were more sensitive to the substituents: COOH or COOEt groups shifted the $\text{Ru}^{\text{III}}/\text{Ru}^{\text{II}}$ couple in a more positive direction and the first reductions with COOEt even more so, whereas the intercession of a phenylene spacer softened these changes, such that the $\text{Ru}^{\text{III}}/\text{Ru}^{\text{II}}$ couple of the **Et1** species matched that of the parent tpy complex. In spite of the fact that *O*-alkyl groups reduce the π -withdrawing ability of the carboxyl $\text{C}=\text{O}$ group, the COOH groups were found to exert a weaker effect than the COOEt groups, part of which was attributable to their acidities, as had been noted in **NH**-acidic cases.^[20,26] In general, the calculated ordering of the frontier orbitals was more faithfully followed by the reduction potentials than by the oxidation potentials, and by the dpp cases than by the tpy analogues. Since the highest-occupied MOs are side chain in origin in those species with phenylene spacers, their oxidations may initially occur on the side chain, but the oxidized forms perhaps relax to lower-energy states that are measured by $E_{1/2}$ values but are not reflected by the MO levels of the unoxidized forms.

Conclusion

The target ligands and complexes were prepared by short routes in good to excellent yields, and were completely characterized. The yields were generally lower in the dpp cases, in part because of decreased stability, greater difficulties in handling and increased levels of side products (and the need for purification).

Bond lengths, bond angles and inter-ring torsions were highly variable in the crystals containing the tpy ligands described in the literature, owing to packing forces and secondary interactions, and comparison with the more consistent DFT-calculated structures was difficult. DFT slightly overestimated the bond lengths but correctly predicted the side-chain conformations. In terms of electronic structures, COOH or COOEt groups were found to act as electron-withdrawing substituents, as expected, but phenylene spacers acted as electron-donating substituents that moderated the effects of COOH or COOEt groups. These structures led to reasonably well-predicted UV/Vis spectra. A notable finding is the intraligand character of the low-energy transitions in the complexes with phenylene spacers, especially when esterified. Although the experimental λ_{MLCT} positions varied little, and were slightly redshifted in the dpp complexes relative to their tpy analogues, the electrochemical potentials were positively shifted in comparison with the tpy analogues, in line with the DFT-predicted frontier orbitals.

It remains to be seen whether the TiO_2 -chemisorbed complexes will more closely resemble the acid or the ester forms studied here, insofar as these show differences in excited-state energies (as reflected by ground-state LUMO levels) and in the quality of the electronic coupling between the semiconductor conduction band and the ligand-centred excited-state HOMO (as reflected by the degree of coplanarity between the side chain and the central pyridine ring).

Phenylene spacers usefully shift the LUMO levels to higher energies but likely diminish the degree of electronic coupling. The localization of the LUMOs over the pyrazine rings in the dpp cases may further hinder effective electronic coupling. Preliminary results on the surface attachment, surface spectral and electrochemical properties and photovoltaic performances of some of the tpy complexes have appeared elsewhere.^[27]

Experimental Section

General: The preparation of ligands Et2 and Et4 is reported elsewhere.^[28] All reagents and solvents were reagent grade and used without further purification, except dry CH₃CN, which was obtained by distillation with P₂O₅ prior to use. The ¹H and ¹³C NMR spectra of ligands and complexes were recorded at room temperature in [D]tfa with an external reference capillary containing D₂O, or in CDCl₃, [D₆]dmsO or CD₃CN, with 300 or 400 MHz Bruker ARZ instruments. Chemical shifts (δ) are reported in parts per million (ppm) downfield from tetramethylsilane (TMS). The resonance assignments were supported by 2D NMR spectroscopic techniques (¹H-¹H COSY, ¹H-¹³C HSQC, ¹H-¹³C HMBC and DEPT-135) and appear in the Supporting Information. Fourier-transform infrared (FTIR) data were obtained by using a Genesis II spectrometer with samples prepared as KBr pellets. UV/Vis spectra were obtained by using an Ultraspec 4300 pro Biochrom spectrometer with samples prepared in dry CH₃CN at 10⁻⁵–10⁻⁶ M. Electrochemical data were obtained with an Autolab Eco-Chemie BV analyzer in a three-electrode cell at room temperature in anhydrous CH₃CN containing 0.1 M *n*Bu₄NPF₆ (TBAH) after purging with N₂ for 15 min. Cyclic voltammograms were obtained with a Pt disk working electrode, a graphite counterelectrode and an Ag/AgCl wire as the pseudoreference electrode. The potentials were scanned from +1.6 to –2 V at rates between 100 and 1000 mV s⁻¹. *E*⁰ values were taken to be the mean of anodic (*E*_{pa}) and cathodic (*E*_{pc}) peak potentials from the tenth steady-state scan at 100 mV s⁻¹, and verified by differential pulse voltammetry. Waves were considered to be reversible if the peak cathodic current (*i*_c) equalled the peak anodic current (*i*_a), and if DPV plots of *i*_c vs. $v^{1/2}$ were linear, in which *v* is the scan rate. The potentials were referenced internally to the ferrocenium/ferrocene couple [*E*(Fc⁺/Fc) = +0.64 V vs. normal hydrogen electrode (NHE) in CH₃CN].^[29] High-resolution EI-MS was performed with a Waters GCT Premier instrument. Matrix-free LDI-MS was carried out with a Voyager-DE spectrometer (PerSeptive Biosystems) equipped with a TOF detector in the positive ion mode. Elemental analyses were performed by weighing samples under N₂ by Guelph Chemical Laboratories (Guelph, ON, Canada).

Computational Details: Geometry-optimized structures were obtained by using Gaussian 03 [G03W C.02 (v6.0)] employing DFT calculations, using the hybrid B3LYP exchange-correlation functional and the LANL2DZ basis set with spin-restricted wave functions for closed-shell species and spin-unrestricted wave functions for open-shell species.^[30] A tight convergence (10–8 a.u.) was used for all calculations. Vibrational frequency calculations were performed on all optimized complexes to verify that an energy minimum had been attained. The wave functions were also checked for stability. All the ground states are spin singlets. The energies of the predicted electronic transitions were obtained by using the TD-DFT method.^[31] The absorption profiles of the complexes were calculated by using the SWIZARD program.^[32] A natural population analysis (G03W) was also carried out.

4'-(4-Carboxyphenyl)-2,2':6',2''-terpyridine (H1): 2-Acetylpyridine (290 mg, 2.4 mmol) and 4-carboxybenzaldehyde (180 mg, 1.2 mmol) were dissolved in CH₃OH (8 mL) by stirring for 5 min, followed by addition of 15% KOH (7.2 mL) and concentrated NH₄OH (0.8 mL). The mixture was allowed to stand at ambient temperature for 3 d. The emulsion formed was filtered off and washed with CHCl₃ (4 mL) and cold CH₃OH/H₂O (1:1; 4 mL). The crude product was suspended in CH₃OH/H₂O (80:20), and the mixture was stirred and sonicated at 35 °C until a clear solution was obtained. This was then acidified to pH = 2 by addition of 1 M HCl, resulting in the formation of a white precipitate that was collected by vacuum filtration and rinsed with cold water. The solid was dried by means of vacuum filtration to give the pure product as a white solid (340 mg, 80%). ¹H NMR ([D]tfa/D₂O capillary): δ = 7.90 (d, 2 H), 8.13 (dd, 2 H), 8.30 (d, 2 H), 8.83 (d, 2 H), 8.65 (dd, 2 H), 8.74 (s, 2 H), 9.04 (d, 2 H) ppm. ¹³C NMR ([D]tfa/D₂O capillary): δ = 126.0, 127.2, 129.8, 130.7, 133.0, 133.9, 143.1, 144.9, 149.1, 149.9, 150.9, 156.9, 174.2 ppm. C₂₂H₁₅N₃O₂ (353.38): calcd. C 74.78, H 4.28, N 11.89; found C 74.71, H 3.99, N 11.38. EI-MS: *m/z* (%) = 353 (100), 336 (2), 325 (8), 308 (24). IR: $\tilde{\nu}$ = 1691 (C=O str.) cm⁻¹.

4'-Carboxy-2,2':6',2''-terpyridine (H2): 2-Acetylpyridine (290 mg, 2.4 mmol) and ethyl glyoxalate (0.238 mL, 1.2 mmol) were used in the same manner as for H1. The crude product was dissolved and acidified as before to give a suspension, which was collected by filtration and carefully washed with a small amount of slightly acidified water and a small amount of cold water. Drying under vacuum provided H2 as the hydrochloride salt, which was a white-tinged pink precipitate containing traces of free HCl (225 mg, 60%). ¹H NMR ([D]tfa/D₂O capillary): δ = 8.53 (dd, 2 H), 9.13 (s, 2 H), 9.21 (d, 2 H), 9.45 (d, 2 H) ppm. ¹³C NMR ([D]tfa/D₂O capillary): δ = 125.1, 125.4, 128.8, 142.7, 143.0, 146.0, 148.5, 148.7, 166.7 ppm. IR: $\tilde{\nu}$ = 1694 (C=O str.) cm⁻¹.

4-(4-Carboxyphenyl)-2,6-dipyrazin-2-ylpyridine (H3): By following the same procedure used for H1, 2-acetylpyridine (295 mg, 2.4 mmol) was used to produce a shiny white, flaky solid (347 mg, 80%). ¹H NMR ([D]tfa/D₂O capillary): δ = 8.36 (d, 2 H), 8.66 (d, 2 H), 9.30 (br. s, 2 H), 9.48 (br., 2 H), 9.77 (s, 2 H), 10.37 (br. s, 2 H) ppm. ¹³C NMR ([D]tfa/D₂O capillary): δ = 123.5, 127.9, 131.2, 131.5, 136.2, 138.5, 140.3, 148.6, 150.4, 157.1, 171.8 ppm. C₂₀H₁₃N₅O₂ (355.35): calcd. C 67.60, H 3.69, N 19.71; found C 67.69, H 3.70, N 19.31. IR: $\tilde{\nu}$ = 1716 (C=O str.), 3422 (O–H str.) cm⁻¹.

4-Carboxy-2,6-dipyrazin-2-ylpyridine (H4): As for H3, 2-acetylpyridine (295 mg, 2.4 mmol) was used to produce a beige solid (180 mg, 55%). ¹H NMR ([D]tfa/D₂O capillary): δ = 8.93 (d, 2 H), 9.37 (br. s, 2 H), 9.54 (d, 2 H), 10.06 (s, 2 H) ppm. ¹³C NMR ([D]tfa/D₂O capillary): δ = 125.1, 133.1, 134.1, 141.3, 149.7, 152.2, 155.6, 168.3 ppm. C₁₄H₉N₅O₂ (279.25): calcd. C 60.21, H 3.25, N 25.08; found C 60.52, H 3.10, N 25.34. EI-MS: *m/z* (%) = 279.15 (100), 262.15 (2), 251.15 (5), 235.14 (12.1). IR: $\tilde{\nu}$ = 1710 (C=O str.) cm⁻¹.

Esterification

4'-(4-Ethoxycarbonylphenyl)-2,2':6',2''-terpyridine (Et1) and 4'-Ethoxycarbonyl 2,2':6',2''-terpyridine (Et3): The crude K⁺/NH₄⁺ salt form of acid H1 or H3 was dissolved in EtOH in the presence of a catalytic amount of H₂SO₄ and heated to reflux for 2.5–3 d. The pure product was isolated as white flakes after extraction with CH₂Cl₂, affording ligands Et1 (yield 70%) or Et3 (yield 76%).

Ester Et1: ¹H NMR (CDCl₃): δ = 1.45 (t, 3 H), 4.44 (q, 2 H), 7.36 (dd, 2 H), 7.88 (dd, 2 H), 7.96 (d, 2 H), 8.18 (d, 2 H), 8.67 (d, 2

H), 8.74 (d, 2 H), 8.76 (s, 2 H) ppm. ^{13}C NMR (CDCl_3): δ = 14.3, 61.1, 118.9, 121.7, 124.0, 127.3, 130.1, 130.8, 136.9, 142.8, 149.1, 149.1, 155.9, 156.1, 166.2 ppm. $\text{C}_{24}\text{H}_{19}\text{N}_3\text{O}_2$ (381.43): calcd. C 75.72, H 5.02, N 11.02; found C 75.72, H 5.18, N 10.90. EI-MS: m/z (%) = 381 (100), 352 (12), 336 (21), 308 (29). IR: $\tilde{\nu}$ = 1690 (C=O str.) cm^{-1} .

Ester Et3: ^1H NMR (CDCl_3): δ = 1.37 (t, 3 H), 4.41 (q, 2 H), 7.93 (d, 2 H), 8.21 (d, 2 H), 8.65 (br. s, 2 H), 8.69 (br. s, 2 H), 8.75 (s, 2 H), 9.88 (br. s, 2 H) ppm. ^{13}C NMR (CDCl_3): δ = 14.3, 61.3, 119.9, 127.2, 130.3, 131.3, 142.0, 143.6, 144.9, 149.7, 150.5, 154.6, 166.1 ppm. $\text{C}_{22}\text{H}_{17}\text{N}_5\text{O}_2$ (383.40): calcd. C 68.92, H 4.47, N 18.27; found C 69.09, H 4.62, N 17.95. EI-MS: m/z (%) = 383.27 (27), 338.27 (5), 284.21 (16.9). IR: $\tilde{\nu}$ = 1726 (C=O str.) cm^{-1} .

Ruthenium Complexes

Bis[4'-(4-Carboxyphenyl)-2,2':6',2''-terpyridine]ruthenium(II) Bis(hexafluorophosphate) [Ru(H1) $_2$](PF $_6$) $_2$: $\text{RuCl}_3 \cdot 3\text{H}_2\text{O}$ (147 mg, 0.56 mmol) and AgBF_4 (330 mg, 1.69 mmol) were dissolved in dmf (30 mL), and the mixture was kept at reflux for 3 h until a sand-colored suspension appeared and the solution had turned bright red. Upon addition of ligand H1 (400 mg, 1.13 mmol), the mixture turned black, at which point more dmf (5 mL) was added, and reflux was maintained for 3 d, yielding a red solution. This was filtered through Celite, and the filtrate was treated with 0.5 M aqueous NH_4PF_6 (18 mL) and allowed to stand at ambient temperature overnight. The red precipitate was isolated by filtration through Celite, rinsed several times with water and twice with diethyl ether, and finally collected with hot CH_3CN containing a few drops of aqueous HPF_6 (60% tech. grade solution). The solution was concentrated, and a red microcrystalline product was obtained after the addition of diethyl ether (590 mg, 95%). ^1H NMR ($[\text{D}_6]\text{dmsO}$): δ = 7.28 (dd, 4 H), 7.56 (d, 4 H), 7.98 (dd, 4 H), 8.29 (d, 4 H), 8.55 (d, 4 H), 9.14 (d, 4 H), 9.54 (s, 4 H) ppm. ^{13}C NMR ($[\text{D}_6]\text{dmsO}$): δ = 121.9, 125.3, 128.2, 128.3, 130.6, 132.5, 138.5, 140.6, 146.1, 152.7, 155.6, 158.3, 167.3 ppm. $\text{C}_{44}\text{H}_{30}\text{F}_{12}\text{N}_6\text{O}_4\text{P}_2\text{Ru}$ (1097.75): calcd. C 48.14, H 2.75, N 7.66; found C 47.53, H 2.70, N 7.45. LDI-MS: m/z (%) = 1097.34 (13), 808.17 (23), 763.17 (32), 718.18 (61). IR: $\tilde{\nu}$ = 1713 (C=O str.), 3431 (O–H str.), 842 (P–F str.) cm^{-1} .

Bis[4'-(4-carboxy-2,2':6',2''-terpyridine)ruthenium(II) Bis(hexafluorophosphate) [Ru(H2) $_2$](PF $_6$) $_2$: Complex $[\text{Ru}(\text{Et}2)_2](\text{PF}_6)_2$ (0.17 mg, 0.17 mmol) was suspended in water (20 mL) to which 0.1 M NaOH (6 mL) was added. The suspension was heated to reflux for 1.5 d. The resulting red solution was concentrated to remove EtOH, then water (4 mL) was added, and the solution was acidified to pH = 2 by addition of 1 M perchloric acid or HCl, resulting in the immediate formation of a precipitate. This was collected by vacuum filtration, then washed with cold water and copiously with diethyl ether to give the pure product as a red powder in 100% yield (160 mg). ^1H NMR ($[\text{D}_6]\text{dmsO}$): δ = 7.19 (dd, 4 H), 7.36 (d, 4 H), 7.96 (dd, 4 H), 8.67 (d, 4 H), 9.25 (s, 4 H) ppm. ^{13}C NMR ($[\text{D}_6]\text{dmsO}$): δ = 123.7, 125.6, 128.4, 138.2, 138.8, 152.7, 155.5, 157.6, 165.9 ppm. $\text{C}_{32}\text{H}_{22}\text{F}_{12}\text{N}_6\text{O}_4\text{P}_2\text{Ru}$ (945.56): calcd. C 40.65, H 2.35, N 8.89; found C 40.09, H 2.38, N 9.17. LDI-MS: m/z (%) = 800.18 (20), 798.17 (80), 583.08 (70), 566.09 (80). IR: $\tilde{\nu}$ = 1694 (C=O str.), 3447 (O–H str.) cm^{-1} .

{Bis[4-(4-carboxyphenyl)-2,6-dipyrazin-2-ylpyridine]}ruthenium(II) Bis(hexafluorophosphate) [Ru(H3) $_2$](PF $_6$) $_2$: Analogously to 4'-(4-carboxyphenyl)-2,2':6',2''-terpyridine,^[5] $\text{RuCl}_3 \cdot 3\text{H}_2\text{O}$ (73 mg, 0.29 mmol), AgBF_4 (163 mg, 0.837 mmol) and ligand H3 (200 mg, 0.563 mmol) were used to obtain a dark red microcrystalline product (307 mg, 58%). ^1H NMR ($[\text{D}_6]\text{dmsO}$): δ = 7.74 (br. s, 4 H), 8.34 (d, 4 H), 8.49 (br. s, 4 H), 8.57 (d, 4 H), 9.72 (s, 4 H), 10.2 (br. s, 4 H) ppm. ^{13}C NMR ($[\text{D}_6]\text{dmsO}$): δ = 122.5, 128.4, 130.7, 133.0,

140.0, 146.0, 147.3, 148.0, 149.0, 153.6, 154.6, 167.4 ppm. $\text{C}_{40}\text{H}_{26}\text{F}_{12}\text{N}_{10}\text{O}_4\text{P}_2\text{Ru}$ (1101.70): calcd. C 43.61, H 2.38, N 12.71; found C 43.82, H 2.13, N 12.25. LDI-MS: m/z (%) = 810.87 (100), 766.90 (100), 722.92 (38). IR: $\tilde{\nu}$ = 1707 (C=O), 3434 (O–H str.), 837 (PF $_6$) cm^{-1} .

[Bis(4-carboxy-2,6-dipyrazin-2-ylpyridine)]ruthenium(II) Bis(hexafluorophosphate) [Ru(H4) $_2$](PF $_6$) $_2$: This was produced in the same manner as was used to obtain bis(4'-carboxy-2,2':6',2''-terpyridine)ruthenium(II) bis(hexafluorophosphate),^[5] by hydrolysis of $[\text{Ru}(\text{Et}4)_2](\text{PF}_6)_2$ (0.171 mg, 0.17 mmol) to produce a red powder (293 mg, 38%). ^1H NMR (CD_3CN): δ = 7.47 (d, 4 H), 8.41 (d, 4 H), 9.43 (s, 4 H), 9.80 (br. s, 4 H) ppm. ^{13}C NMR ($[\text{D}_6]\text{dmsO}$): δ = 124.7, 139.5, 145.8, 148.0, 148.7, 152.9, 154.7, 165.7 ppm. $\text{C}_{28}\text{H}_{18}\text{F}_{12}\text{N}_{10}\text{O}_4\text{P}_2\text{Ru}$ (949.51): calcd. C 35.42, H 1.91, N 14.75; found C 35.22, H 2.22, N 14.42. LDI-MS: m/z (%) = 803.14 (50), 587.06 (40), 570.07 (95). IR: $\tilde{\nu}$ = 1712 (C=O str.), 838 (P–F str.) cm^{-1} .

Bis[4'-(4-ethoxycarbonylphenyl)-2,2':6',2''-terpyridine]ruthenium(II) Bis(hexafluorophosphate) [Ru(Et1) $_2$](PF $_6$) $_2$: By following the same procedure used for $[\text{Ru}(\text{H}1)_2](\text{PF}_6)_2$, but without the use of HPF_6 , $\text{RuCl}_3 \cdot 3\text{H}_2\text{O}$ (172 mg, 0.655 mmol), AgBF_4 (383 mg, 1.97 mmol) and ligand Et1 (500 mg, 1.13 mmol) were converted to complex $[\text{Ru}(\text{Et}1)_2](\text{PF}_6)_2$, a red microcrystalline product (0.74 g, 98%). ^1H NMR (CD_3CN): δ = 1.48 (t, 6 H), 4.48 (q, 4 H), 7.22 (dd, 4 H), 7.46 (d, 4 H), 7.99 (t, 4 H), 8.33 (d, 4 H), 8.40 (d, 4 H), 8.68 (d, 4 H), 9.07 (s, 4 H) ppm. ^{13}C NMR (CD_3CN): δ = 13.6, 61.3, 121.9, 124.6, 127.5, 128.0, 130.3, 132.1, 138.1, 141.0, 147.0, 152.5, 155.5, 158.0, 165.7 ppm. $\text{C}_{48}\text{H}_{38}\text{F}_{12}\text{N}_6\text{O}_4\text{P}_2\text{Ru}$ (1153.86): calcd. C 49.96, H 3.32, N 7.28; found C 49.54, H 3.30, N 6.99. LDI-MS: m/z (%) = 1153.28 (13), 863.22 (22), 835.18 (12), 807.16 (80). IR: $\tilde{\nu}$ = 1712 (C=O str.), 838 (P–F str.) cm^{-1} .

Bis[4'-(4-ethoxycarbonyl)-2,2':6',2''-terpyridine]ruthenium(II) Bis(hexafluorophosphate) [Ru(Et2) $_2$](PF $_6$) $_2$: As for $[\text{Ru}(\text{Et}1)_2](\text{PF}_6)_2$, $\text{RuCl}_3 \cdot 3\text{H}_2\text{O}$ (85 mg, 0.325 mmol), AgBF_4 (191 mg, 0.98 mmol) and ligand Et2 (200 mg, 0.655 mmol) were converted to $[\text{Ru}(\text{Et}2)_2](\text{PF}_6)_2$, also a red microcrystalline product (269 mg, 82%). ^1H NMR (CD_3CN): δ = 1.59 (t, 3 H), 4.68 (q, 2 H), 7.21 (dd, 4 H), 7.37 (d, 4 H), 7.98 (dd, 4 H), 8.69 (d, 4 H), 9.24 (s, 4 H) ppm. ^{13}C NMR (CD_3CN): δ = 13.6, 62.9, 122.8, 125.0, 127.8, 138.4, 138.4, 152.5, 155.7, 157.3, 164.8 ppm. $\text{C}_{36}\text{H}_{30}\text{F}_{12}\text{N}_6\text{O}_4\text{P}_2\text{Ru}$ (1001.67): calcd. C 43.17, H 3.02, N 8.39; found C 43.20, H 3.08, N 8.42. LDI-MS: m/z (%) = 782.83 (100), 711.83 (100), 684.86 (43), 639.85 (100), 611.95 (98), 566.88 (86). IR: $\tilde{\nu}$ = 1727 (C=O str.), 843 (P–F str.) cm^{-1} .

{Bis[4-(4-ethoxycarbonylphenyl)-2,6-dipyrazin-2-ylpyridine]}ruthenium(II) Bis(hexafluorophosphate) [Ru(Et3) $_2$](PF $_6$) $_2$: $\text{RuCl}_3 \cdot 3\text{H}_2\text{O}$ (137 mg, 0.52 mmol), AgBF_4 (305 mg, 1.56 mmol) and Et3 (400 mg, 1.04 mmol) were used by following the same procedure as with ligand H3. The crude, dark red-brown hexafluorophosphate salt was purified by preparatory TLC on 2 mm-thick Macherey–Nagel Polygram Sil G/UV silica gel plates, developed with CH_3CN /saturated $\text{KNO}_3/\text{H}_2\text{O}$ (65:2:1). The most mobile red band was scraped off and extracted with CH_3CN and CH_3OH . The solvents were evaporated in vacuo. The resulting dark red solid was dissolved in a minimum amount of CH_3CN and poured into a saturated aqueous solution of NH_4PF_6 . The mixture was allowed to stand at ambient temperature overnight to give a red precipitate, which was isolated by vacuum filtration through a Celite layer and washed with cold water and copiously with diethyl ether (180 mg, 30%). ^1H NMR (CD_3CN): δ = 1.48 (t, 6 H), 4.49 (q, 4 H), 7.56 (s, 4 H), 8.37 (d, 4 H), 8.42 (br. s, 4 H), 8.44 (d, 4 H), 9.25 (s, 4 H), 9.80 (br. s, 4 H) ppm. ^{13}C NMR (CD_3CN): δ = 13.6, 61.4, 123.0,

128.1, 130.5, 133.0, 140.0, 145.0, 147.6, 148.3, 149.0, 153.1, 154.3, 165.8 ppm. $C_{44}H_{34}F_{12}N_{10}O_4P_2Ru$ (1157.81): calcd. C 45.64, H 2.96, N 12.10; found C 45.54, H 3.28, N 11.94. LDI-MS: m/z (%) = 939.7 (100), 866.75 (100), 839.74 (30). IR: $\tilde{\nu}$ = 1708 (C=O str.), 846 (P–F str.) cm^{-1} .

[Bis(4-ethoxycarbonyl-2,6-dipyrazin-2-ylpyridine)]ruthenium(II) Bis(hexafluorophosphate) [Ru(Et4)₂(PF₆)₂]: This was prepared in the same way as [Ru(H3)₂](PF₆)₂ by using RuCl₃·3H₂O (213 mg, 0.814 mmol), AgBF₄ (476 mg, 2.44 mmol) and ligand Et4 (500 mg, 1.63 mmol) to give a red microcrystalline product (350 mg, 38%). ¹H NMR (CD₃CN): δ = 1.56 (t, 6 H), 4.72 (q, 4 H), 7.44 (dd, 4 H), 8.39 (d, 4 H), 9.41 (s, 4 H), 9.75 (d, 4 H) ppm. ¹³C NMR (CD₃CN): δ = 13.6, 63.2, 124.1, 139.1, 145.4, 147.7, 148.6, 152.4, 154.6, 163.3 ppm. $C_{32}H_{26}F_{12}N_{10}O_4P_2Ru$ (1005.62): calcd. C 38.22, H 2.61, N 13.93; found C 38.35, H 2.73, N 13.59. LDI-MS: m/z (%) = 714.94 (100), 687.97 (43). IR: $\tilde{\nu}$ = 1724 (C=O str.), 834 (P–F str.) cm^{-1} .

Supporting Information (see footnote on the first page of this article): ¹H and ¹³C NMR spectroscopic assignments and coupling constants; 1D and 2D NMR spectra; mass spectral assignments; frontier molecular orbital compositions; experimental and predicted optical spectra; transition assignments for near-UV and visible absorptions; cyclic and differential pulse voltammograms; selected orbital images and orbital difference diagrams; tables of atomic charges from natural population analysis; and MOL2 coordinates for all geometry-optimized complexes.

Acknowledgments

We thank the Natural Sciences and Engineering Research Council (Canada) for funding, Professor A. B. P. Lever for helpful discussions, Professor S. Morin for help with the electrochemical work, and Wylie O, Dr. G. Koyanagi and D. Kalinina for the DFT calculations.

- [1] P. G. Potvin, P. U. Luyen, J. Bräckow, *J. Am. Chem. Soc.* **2003**, *125*, 4894–4906.
- [2] M. W. Cooke, G. S. Hanan, F. Loiseau, S. Campagna, M. Watanabe, Y. Tanaka, *J. Am. Chem. Soc.* **2007**, *129*, 10479–10488.
- [3] E. C. Constable, E. L. Dunphy, C. E. Housecroft, M. Neuburger, S. Schaffner, F. Schapera, S. R. Batten, *Dalton Trans.* **2007**, 4323–4332.
- [4] M. Graetzel, *J. Photochem. Photobiol. C: Photochem. Rev.* **2003**, *4*, 145–153.
- [5] F. Barigelletti, L. Flamigni, V. Balzani, J.-P. Collin, J.-P. Sauvage, A. Sour, E. C. Constable, A. M. W. Cargill Thompson, *J. Chem. Soc., Chem. Commun.* **1993**, 942–944.
- [6] M. Graetzel, *Energy Resources through Photochemistry and Catalysis*, Academic Press, New York, NY, USA, **1983**.
- [7] L. J. Nurkkala, R. O. Steen, H. K. J. Friberg, J. A. Haegstroem, P. V. Bernhardt, M. J. Riley, S. J. Dunne, *Eur. J. Inorg. Chem.* **2008**, 4101–4110.
- [8] R. J. Crutchley, A. B. P. Lever, *J. Am. Chem. Soc.* **1980**, *102*, 7128–7129.
- [9] R. Liegghio, P. G. Potvin, A. B. P. Lever, *Inorg. Chem.* **2001**, *40*, 5485–5486.
- [10] F. A. Mutlaq, P. G. Potvin, A. I. Philippopoulos, P. Falaras, *Eur. J. Inorg. Chem.* **2007**, 2121–2128.
- [11] N. A. Anderson, T. Lian, *Coord. Chem. Rev.* **2004**, *248*, 1231–1246.
- [12] G. D. Storrier, S. B. Colbran, *Inorg. Chim. Acta* **1999**, *284*, 76–84.
- [13] F. Neve, M. La Deda, F. Puntoriero, S. Campagna, *Inorg. Chim. Acta* **2006**, *359*, 1666–1672.
- [14] H. Wolpher, S. Sinha, J. Pan, A. Johansson, M. J. Lundqvist, P. Persson, R. Lomoth, J. Bergquist, L. Sun, V. Sundström, B. Åkermark, T. Polívka, *Inorg. Chem.* **2007**, *46*, 638–651.
- [15] E. Figgemeier, V. Aranyos, E. C. Constable, R. W. Handel, C. E. Housecroft, C. Risinger, A. Hagfeldt, E. Mukhtar, *Inorg. Chem. Commun.* **2004**, *7*, 117–121.
- [16] S. Vadvuescu, P. G. Potvin, *Eur. J. Inorg. Chem.* **2004**, 1763–1769.
- [17] M. Abboud, D. Kalinina, P. G. Potvin, *Inorg. Chim. Acta* **2009**, *362*, 4953–4959.
- [18] R.-A. Fallahpour, *Synthesis* **2000**, 1138–1142.
- [19] J. Husson, M. Beley, G. Kirsch, *Tetrahedron Lett.* **2003**, *44*, 1767–1770.
- [20] J. Zadykiewicz, P. G. Potvin, *Inorg. Chem.* **1999**, *38*, 2434.
- [21] P. G. Potvin, P. U. Luyen, F. Al-Mutlaq, *New J. Chem.* **2001**, *25*, 839–846.
- [22] J. Zadykiewicz, P. G. Potvin, *J. Coord. Chem.* **1999**, *47*, 395–407.
- [23] D. E. Morris, K. W. Hanck, M. K. DeArmond, *J. Electroanal. Chem.* **1983**, *149*, 115–130.
- [24] C. R. Hecker, A. K. I. Gushurst, D. R. McMillin, *Inorg. Chem.* **1991**, *30*, 538–541.
- [25] R. J. Crutchley, A. B. P. Lever, *Inorg. Chem.* **1982**, *21*, 2276–2282.
- [26] Y. Luo, P. G. Potvin, Y.-H. Tse, A. B. P. Lever, *Inorg. Chem.* **1996**, *35*, 5445–5452.
- [27] A. Sephehrifard, A. Stublla, S. Haftchenary, S. Chen, P. G. Potvin, S. Morin, *J. New Mater. Electrochem. Syst.* **2008**, *11*, 281–285.
- [28] G. C. Vougioukalakis, T. Stergiopoulos, G. Kantonis, A. G. Kontos, K. Papadopoulos, A. Stublla, P. G. Potvin, F. Falaras, manuscript in preparation.
- [29] G. N. Connelly, E. W. Geiger, *Chem. Rev.* **1996**, *96*, 877–910; J. R. Aranzaes, M. C. Daniel, D. Astruc, *Can. J. Chem.* **2006**, *84*, 288–299.
- [30] M. J. Frisch, G. W. Trucks, H. B. Schlegel, G. E. Scuseria, M. A. Robb, J. R. Cheeseman, J. A. Montgomery Jr., T. Vreven, K. N. Kudin, J. C. Burant, J. M. Millam, S. S. Iyengar, J. Tomasi, V. Barone, B. Mennucci, M. Cossi, G. Scalmani, N. Rega, G. A. Petersson, H. Nakatsuji, M. Hada, M. Ehara, K. Toyota, R. Fukuda, J. Hasegawa, M. Ishida, T. Nakajima, Y. Honda, O. Kitao, H. Nakai, M. Klene, X. Li, J. E. Knox, H. P. Hratchian, J. B. Cross, V. Bakken, C. Adamo, J. Jaramillo, R. Gomperts, R. E. Stratmann, O. Yazyev, A. J. Austin, R. Cammi, C. Pomelli, J. W. Ochterski, P. Y. Ayala, K. Morokuma, G. A. Voth, P. Salvador, J. J. Dannenberg, V. G. Zakrzewski, S. Dapprich, A. D. Daniels, M. C. Strain, O. Farkas, D. K. Malick, A. D. Rabuck, K. Raghavachari, J. B. Foresman, J. V. Ortiz, Q. Cui, A. G. Baboul, S. Clifford, J. Cioslowski, B. B. Stefanov, G. Liu, A. Liashenko, P. Piskorz, I. Komaromi, R. L. Martin, D. J. Fox, T. Keith, M. A. Al-Laham, C. Y. Peng, A. Nanayakkara, M. Challacombe, P. M. W. Gill, B. Johnson, W. Chen, M. W. Wong, C. Gonzalez, J. A. Pople, *Gaussian 03* (G03W revision C.02), Gaussian, Inc., Wallingford, CT, **2004**.
- [31] S. Grimme, *Rev. Comput. Chem.* **2004**, *20*, 153–218.
- [32] S. I. Gorelsky, *SWizard program*, CCR1, University of Ottawa, Ottawa, Canada, **2008**, <http://www.sg-chem.net/>.

Received: February 3, 2010
Published Online: May 12, 2010